Orbital dynamics in the Tevatron double helix.

LEO MICHELOTTI and SELCUK SARITEPE
Fermilab*, P.O.Box 500, Batavia, IL 60510

A key feature of the Tevatron upgrade is the placement of proton and anti-proton bunches on the branches of a double helix which winds around the current closed orbit. Electrostatic separators will transfer the bunches on and off the double helix so that they experience head-on collisions only at the experimental areas, B0 and D0, all other encounters occurring at large transverse separation. In this way the number of bunches, and the luminosity, can be increased without a proportional growth in the beam-beam tune shift. The scenario raises a number of beam dynamics (*viz.* stability) issues, especially (a) the consequences of sampling magnetic fields far from the magnets' center lines, and (b) the effects of the long-range beam-beam interaction. This report presents the results of (admittedly incomplete) calculations and simulations done to date to explore (b); a Fermilab team (including Ernie Malamud, Glenn Goderre, Norman Gelfand, Gerry Jackson, and many others) have been studying (a), both experimentally and theoretically, but we shall not review those efforts here. The constraint of a page limit has forced us to bound this discussion rather stringently, but a more complete paper will be available as a Fermilab Technical Memo.

1 A model.

Modelling is the art of simplifying until one reaches a problem that has a chance of being solved and perhaps — dare we hope? — understood. Some of the particular simplifications made for these first calculations were:

Lattices and Separators
Calculations were carried out using two low-beta (50 cm β^*) Tevatron lattices designed by Tom Collins and Karl Koepke. The first is an old (September 23, 1987) lattice with horizontal and vertical tunes placed almost exactly at 20.6; we shall refer to it as the "resonant" lattice. The second is more recent (September 27, 1988), and its tunes are shifted slightly to $\nu_x = 20.578$ and $\nu_y = 20.590$; we shall refer to it as the "nonresonant" lattice. The most significant simplification is the neglect of all magnetic field nonlinearities. The locations and excitations of the twelve electrostatic separators were specified by Ernie Malamud; typically, these range from a few to about 20-30 μrad.[4]

Bunch configuration
Calculations were done using a configuration of *evenly spaced* bunches: in particular, we used a set of 21 × 21 bunches, as this number was both a multiple of 3, which assured collisions at both B0 and D0, and a factor of 1113, the number of available buckets.

Beam-beam interaction
Montague's expression for the form of the beam-beam kick, based on a round or elliptic transverse distribution of particles, has been derived in many places, including Evans[1], Gluckstern[3], and Furman[2]. For the calculations described in this paper, the charge distribution in each bunch was taken to be circular gaussian. All calculations were carried out using a "weak-strong" (or "large-small") approximation. There was thus a distinction between "probe" particles and "source" bunches, or macro-particles, the former having no effect on the latter. The source bunch width was recalculated at each collision site, and a nominal 24π mm-mr invariant emittance was assumed throughout, in most, but not all, of the calculations the source bunches contained 6×10^{10} particles each.

Longitudinal momentum
We assume the energy to be 1 TeV; the lattice contains dispersion and natural chromaticity, but it is assumed that $\delta p = 0$.

2 Linearized Dynamics

We discuss in this section results for small amplitude orbits, those which literally are infinitesimally close to the closed orbit. Exploration of moderate to large amplitude orbits will be described in the next section.

*Operated by the Universities Research Association, Inc. under contract with the U.S. Department of Energy.

2.1 The closed orbit.

The electrostatic kicks are designed to position proton and anti-proton bunches on helical orbits while maintaining head-on collisions at B0 and D0. At full separator excitation the spacing between the two branches of the double helix is approximately 6 mm over most of the ring, roughly a 10σ separation for an invariant emittance of $\approx 20\pi$ mm-mr. This separation is displayed, for the nonresonant lattice, in Fig.(1). However, this "bare" orbit

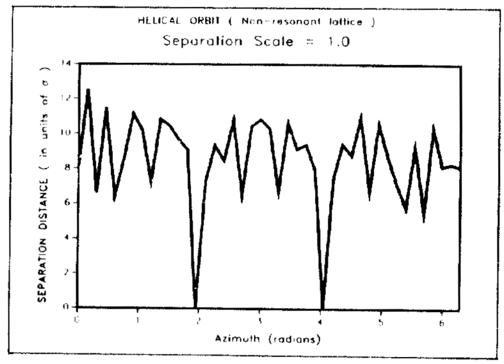

Figure 1: Orbit separation for the model's design orbits.

does not take into account the kicks arising from the long range beam-beam interaction, which distort it into a new, "clothed" orbit.[1] This is, it is hoped, a small effect, but one which may be significant if the transverse excursions of the closed orbit at the experimental areas, B0 and D0, are comparable to the transverse bunch width.

The "clothed" orbit of the model was calculated, via Newton's method, as a fixed point of the single-turn mapping. The Jacobian of the mapping, which is required by Newton's method, was automatically computed using a C++ implementation of "differential" algebra variables.[5] The resulting transverse coordinates of the "clothed" orbit at the B0 interaction region is shown in Figure 2. The ordinate has been scaled by the beamwidth, but this

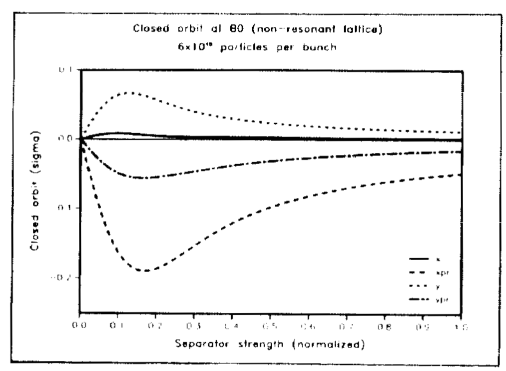

Figure 2: Clothed orbit at B0 .

is *not* meant to imply that the effect scales accordingly; one sigma (which is about 50 μm here) is simply a useful size with which to compare the offsets. The abscissa measures λ_{sep}, the normalized strength of the separators: 0 corresponds to turning them off, and thus having no p$\bar{\text{p}}$ bunch separation; 1 corresponds to the full kicks producing the "bare" closed orbit shown in Figure 1. Notice that at B0, the motion is essentially all vertical for both lattices tested. The size of the displacement is about the same at both locations and smaller than 0.1σ, about 5 μm, over the full range of separator strength. For $\lambda_{sep} > 0.5$ the closed orbit distortion is already smaller than

[1] Not to be confused with a closed orbit calculated in LISP.

$\approx 0.02\sigma \approx 1\mu m$. These deviations are small enough so that one need not compensate for them.

The curve labelled "xpr" actually represents the normalized quantity $\alpha x + \beta x'$, and similarly for the one labelled "ypr"; the limiting value for both of these is a nominal 0.05σ, or less.

2.2 Beam-beam tune shift

By finding the eigenvalues of the Jacobian matrix used to calculate the "clothed" orbit we obtain as a bonus the *exact* tunes of small amplitude motion about the closed orbit. With separators off, the approximate tune shift per beam-beam interaction is given by the usual formula, $\xi \approx 0.007\, N[10^{10}]/\epsilon_{inv}[\pi \text{mm} - \text{mr}]$. This must be multiplied by the number of encounters: for our model 21 × 21 configuration (i.e., 42 hits) with 10^{11} particles per bunch and $\epsilon_{inv} = 24$, we get $\xi \approx 0.13$. The tunes associated with small amplitude oscillations about the closed orbit drop rapidly as separators are turned on. In Figure 3 are plotted the eigentunes associated with the nonresonant lattice with **ppb** $= 6 \times 10^{10}$. The principal feature of

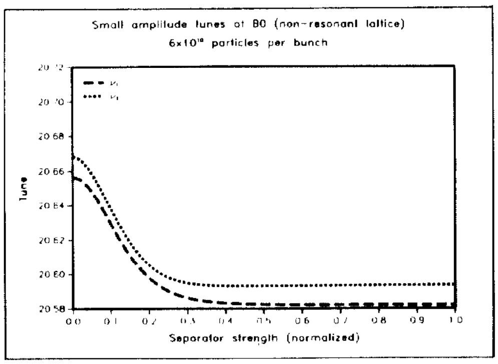

Figure 3: Effect of increasing bunch separation on tune shifts: nonresonant lattice.

these curves is their very rapid falloff, a characteristic observed in Figure 2 as well; the limiting values are attained for $\lambda_{sep} \geq 0.4-0.5$, i.e., with separators powered to ≈ 40-50% of their designed strength.

3 Nonlinear dynamics

Going beyond the linearized model, we explored the tunes of particles on larger amplitude orbits by the simple expedient of plotting the "power" spectra obtained by evaluating FFTs of the orbits. Prior to taking the FFT, the data were multiplied by a windowing function (the Welch window) in order to reduce the diffraction-like effects arising from a finite sample size.[7, pp.441ff] Initial conditions shown were chosen by setting $w_1 = w_2 = w_3 = 0$ and letting w_0 ranging from 0.5 to 5; **ppb** is fixed at 6×10^{10}. Coordinates $\underline{w} = (w_0, w_1, w_2, w_3)$ are interpreted $w_0\sigma \equiv x$, $w_1\sigma \equiv \alpha_x x + \beta_x x'$, $w_2\sigma \equiv y$, and $w_3\sigma \equiv \alpha_y y + \beta_y y'$. Figure 4 illustrates the (limited) amplitude dependence of the tune for a variety of values of λ_{sep} (labelled as **sc** in the figure). The strong amplitude dependence of the tune is suppressed very quickly by

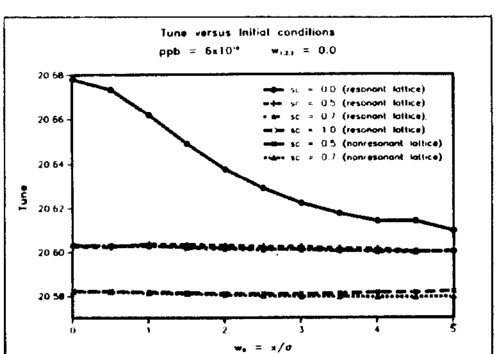

Figure 4: Tune versus initial amplitude for fixed **ppb**.

powering the separators. (Connecting the first two sample points with a straight line segment is a little misleading: of course, the slope of the curve approaches 0 as $x \to 0$.)

Finally, we explored a collection of orbits at both moderate and large amplitudes using the EOA (Exploratory Orbit Analysis) graphics shell AESOP.[6] We shall describe a few of these here, but static, two-dimensional pictures do not convey the full experience of viewing these orbits as they develop in (projected) four dimensions.

A few representative runs at moderate amplitudes are logged in Figures 5. This figure tracks the behavior of an orbit passing through a given point in phase space as λ_{sep}, the normalized separator strength, increases from 0 to 0.5; **ppb** was set at 10^{11}. The calculations for these figures were carried out using the nonresonant lattice. For each value of λ_{sep} we display four phase

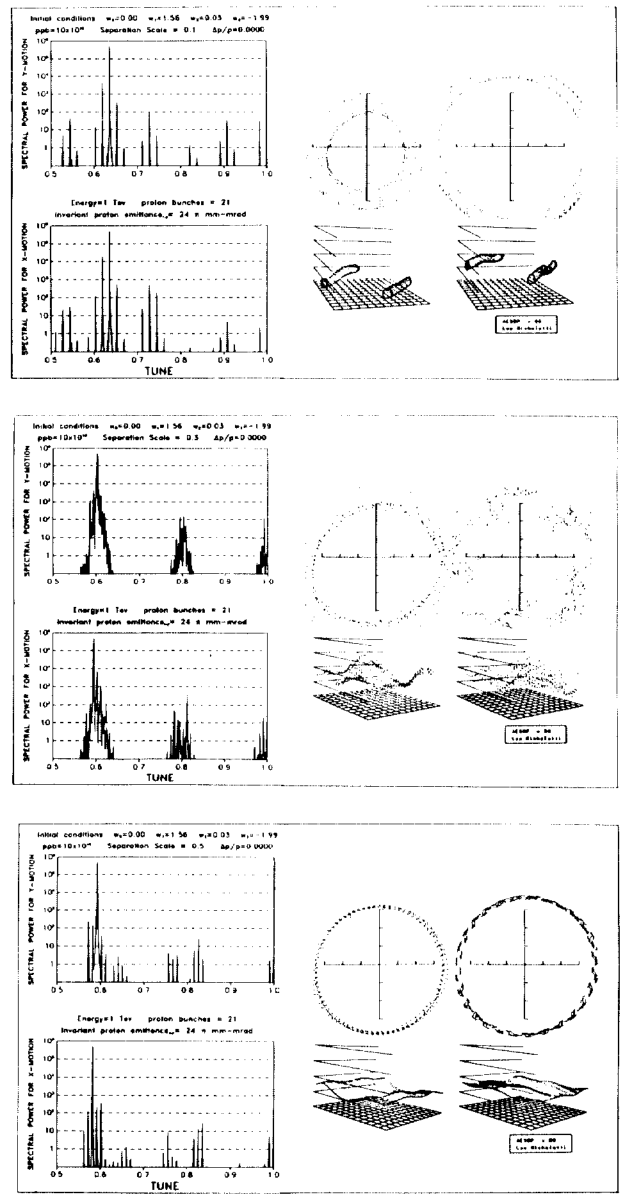

Figure 5: Effects of helical separation.

space projections of the (four-dimensional) orbit and the spectra for horizontal and vertical coordinates. The two-dimensional projections are along the horizontal, (w_0, w_1), and the vertical, (w_2, w_3), coordinates. The coordinates for the three dimensional projections, which we shall refer to as $\delta\delta I$ plots, are the horizontal and vertical "angle" variables and an "action" variable, horizontal action in the left hand plots and vertical in the right. These variables are those obtained by expressing the two-dimensional projections in polar coordinates rather than Cartesian, actions being equivalent to radius squared.

As you scan through Figure 5a-c notice the change from clean, smooth KAM tori when $\lambda_{sep} \leq 0.2$ through a chaotic layer for $\lambda_{sep} \approx 0.3$, and returning to regular behavior when $\lambda_{sep} \geq 0.4$. Observe the increasing complexity of the power spectra as λ_{sep} increases and the orbit approaches a chaotic condition. This broadband "noise" is typical of chaotic behavior. Conversely, as the chaotic layer passes the orbit and it settles down to smooth torus once again, the spectrum becomes once more discrete.[2] One *very* intriguing feature emerges when you compare the spectra from all similar figures which are not shown here due to page limitations. Notice that the peak spectral component shifts with increasing λ_{sep}, as is reasonable, and that the chaotic layer at $\lambda_{sep} = 0.3$ is correlated with (a) the peak spectral component hitting the value 0.6 and (b) a second strong, noisy spectral component coming into existence at 0.8. This suggests a locking onto the $\nu_x = \nu_y = 3/5$ resonance separatrix as the mechanism of chaos, with a possible interference from the $\nu_x = \nu_y = 4/5$ or $2/5$ separatrix as well.

However, large amplitude orbits can experience a different phenomenon, one which is best described in textilic terms: what happens is as though KAM tori were literally woven from threads which unravel and become entangled. To see this happening, we shall track the behavior of the orbit passing through $w = (3,0,0,3)$ as the normalized separator strength, λ_{sep}, is increased from 0.0 to 0.5. This set of calculations were carried out using the resonant lattice. The corresponding $\delta\delta I$ plots are shown in Figure 6. The first plot shows a separatrix for $\lambda_{sep} = 0$; ppb has been set to 10^{11};

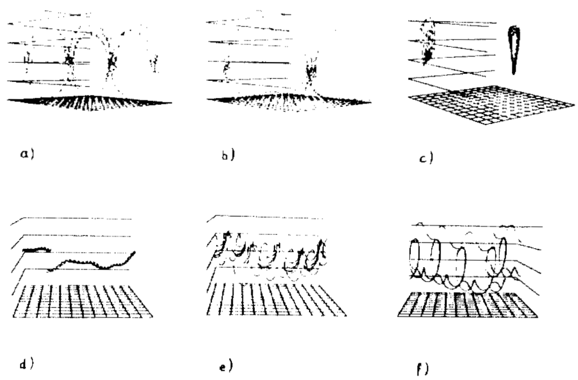

Figure 6: As tori unravel orbits become tangled.

those who think this is too large can rescale by decreasing ϵ_{inv}. The orbit, which is in the vicinity of a $2\nu_x - 2\nu_y$ separatrix, is chaotic and visits both sides of the separatrix. (Bear in mind that what we are viewing is only one three-dimensional slice through the full separatrix.) A remarkable transition occurs as λ_{sep} increases from 0.0 to 0.1; Figure(6b) shows the orbit at $\lambda_{sep} = 0.1$. The separatrix now contains only two lobes rather than the four that it previously had; it looks more like a $\nu_x - \nu_y$ separatrix. It is almost as though one of the unstable resonant orbits defining the separatrix has undergone a transition to stability. (Are we observing here some four-dimensional form of period doubling?) At $\lambda_{sep} \approx 0.14$ another remarkable jump occurs, and the orbit fills the wedge formed by the separatrix, as seen in Figure (6c). The "wedge" smooths out and becomes tighter until, at $\lambda_{sep} \approx 0.3$, as seen in Figure (6d), it winds around a tight KAM torus, close to a stable resonant orbit. (Note the change in viewing angle.) Although it is difficult to tell from these figures, this torus lies remarkably precisely in the intersection region of the separatrix of Figure(6b) or, equivalently, at the cusp of the wedge in Figure (6c). If we now increase λ_{sep} further, an extraordinary thing happens: the torus gets larger and *begins to unravel*. This is seen in Figure(6e), which shows the orbit at $\lambda_{sep} = 0.4$. The unravelling has begun, but enough of shape of the torus remains that one can make out its former existence and location. By $\lambda_{sep} = 0.5$ the torus has completely disappeared and the orbit is simply a tangled thread, as seen in Figure(6e). Here we have a phenomenon due to the long range beam-beam interaction which does not vanish for $\lambda_{sep} > 0.5$. These very large amplitude orbits are still feeling the effect of the source bunches. Keep in mind, however, that we have displayed only the orbits passing through one particular point in phase space. Not all large amplitude orbits behave like this. Indeed, the orbit passing through $(3,0,0,-3)$ still lies on an identifiable, perfectly regular torus. Thus, the problem is (a) to identify the probability of actually encountering such orbits, and (b) understand their impact on stability. This particular tangled orbit, for example remained bounded for over 50,000 iterations. Though it looks ugly, this aesthetic judgement may have no relevance to issues of stability.

[2] I am curious about how these orbits would "sound" if we could convert these spectra into audible sound waves. Is it possible that the ear could discriminate between chaotic and regular behavior better than the eye?

Some large amplitude orbits exhibit phaselock, as seen, for example, in Figure 7. This orbit (resonant lattice) spends most of its history with horizontal and vertical phases locked near $\delta_1 - \delta_2 \approx 0$, or π, resulting in the vertical walls appearing in the $\delta\delta I$ projections. The transitions between

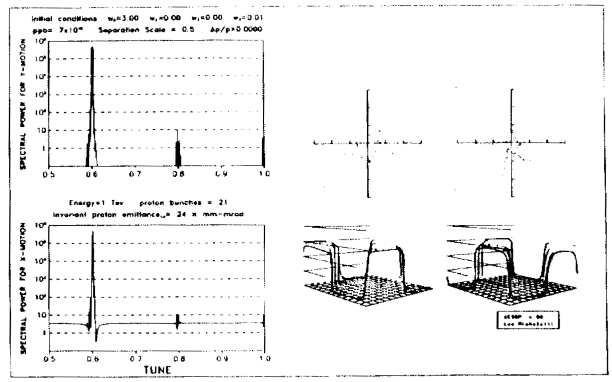

Figure 7: Phaselocked orbit.

these two walls take place on time scales small compared to the time spent in the locked regions.

References

[1] Lynn R. Evans. *The Beam-Beam Interaction*. Technical Report, European Organization for Nuclear Research, 1983. CERN SPS/83-38.

[2] Miguel A. Furman. *Practical Approximations for the Electric Field of Elliptical Beams*. Technical Report, Lawrence Berkeley Laboratory, 1987. SSC-N-312.

[3] Robert Gluckstern. *Scalar Potential for Charge Distributions with Ellipsoidal Symmetry*. Technical Report, Fermi National Accelerator Laboratory, 1986. Fermilab TM-1402.

[4] Ernie Malamud. An electrostatic separator scheme for the tevatron. September 1, 1987 (unpublished).

[5] Leo Michelotti. Differential algebras without differentials: an easy c++ implementation. This Conference.

[6] Leo Michelotti. Exploratory orbit analysis. This Conference.

[7] William H. Press, Brian P. Flannery, Saul A. Teukolsky, and William T. Vettering. *Numerical Recipes in C*. Cambridge University Press, New York, 1988.